

Multiple variability time-scales of the early nitrogen-rich Wolf-Rayet star WR 7

J. A. Toalá¹★, D. M. Bowman², T. Van Reeth², H. Todt³, K. Dsilva², T. Shenar², G. Koenigsberger⁴, S. Estrada-Dorado¹, L. M. Oskina³ and W.-R. Hamann³

¹*Instituto de Radioastronomía y Astrofísica, UNAM Campus Morelia, Apartado postal 3-72, 58090 Morelia, Michoacán, Mexico*

²*Institute of Astronomy, KU Leuven, Celestijnenlaan 200D, 3001 Leuven, Belgium*

³*Institute for Physics and Astronomy, Universität Potsdam, Karl-Liebknecht-Str. 24/25, D-14476 Potsdam, Germany*

⁴*Instituto de Ciencias Físicas, Universidad Nacional Autónoma de México, Ave. Universidad s/n, Chamilpa, Cuernavaca, Mexico*

24 May 2022

ABSTRACT

We present the analysis of the optical variability of the early, nitrogen-rich Wolf-Rayet (WR) star WR 7. The analysis of multi-sector *Transiting Exoplanet Survey Satellite* (TESS) light curves and high-resolution spectroscopic observations confirm multi-periodic variability that is modulated on time-scales of years. We detect a dominant period of 2.6433 ± 0.0005 d in the TESS sectors 33 and 34 light curves in addition to the previously reported high-frequency features from sector 7. We discuss the plausible mechanisms that may be responsible for such variability in WR 7, including pulsations, binarity, co-rotating interacting regions (CIRs) and clumpy winds. Given the lack of strong evidence for the presence of a stellar or compact companion, we suggest that WR 7 may pulsate in quasi-coherent modes in addition to wind variability likely caused by CIRs on top of stochastic low-frequency variability. WR 7 is certainly a worthy target for future monitoring in both spectroscopy and photometry to sample both the short ($\lesssim 1$ d) and long ($\gtrsim 1000$ d) variability time scales.

Key words: stars: evolution — stars: atmospheres — stars: winds, outflows — stars: Wolf-Rayet — stars: individual: WR 7

1 INTRODUCTION

Wolf-Rayet (WR) stars represent one of the most advanced stages of massive stellar evolution. They are H-depleted stars characterised by the presence of broad emission lines from highly ionised species of He, C, N, and O in their spectra (see, e.g., Crowther 2007). WR stars are also distinguished by fast and strong winds (mass-loss rates $\dot{M} \approx 10^{-5} M_{\odot} \text{ yr}^{-1}$, terminal wind velocities $v_{\infty} \approx 2000\text{--}3000 \text{ km s}^{-1}$; e.g., Hamann et al. 2006, 2019, and references therein) which renders them the hot stars with the most powerful winds.

The current formation scenario of WR stars is twofold. It has been proposed that single massive stars with initial mass $M_i \geq 20 M_{\odot}$ might lose up to half their initial masses via slow and dense winds when evolving through a red supergiant (RSG) or eruptive ejections through a luminous blue variable (LBV) phase (Weis 2001; Humphreys 2010). It is argued that this process is able to peel off the outer H-rich layers, leaving behind a classical WR star (Conti 1975). According to the second scenario, first proposed by Paczyński (1967), mass transfer between binary components (Packet 1981; de Mink et al. 2013) could cause stripping of the H-rich envelope, a scenario which has recently gained impetus when it was shown that the majority of massive stars evolve in binary systems (e.g., Vanbeveren et al. 1998; Foellmi et al. 2003; Sana et al. 2012; Sota et al. 2014).

The binary evolutionary channels have interesting implications,

for example, extending the life times of the mass-donors and reducing the initial mass necessary to form a WR star. Nevertheless, the dominance of one scenario over the other has not been demonstrated (e.g., Neugent & Massey 2014; Shenar et al. 2016, 2020), and a third scenario in which a high internal mixing efficiency eventually leads to a He-rich, non-stripped star cannot be excluded (Brott et al. 2011; Hainich et al. 2015).

As the progenitors of neutron stars (NSs) and black holes (BHs), WR stars in binaries offer indispensable laboratories to study the evolution and formation of high-mass X-ray binaries (HMXBs) and BH merger events (Abbott et al. 2019). In this context, it is important to investigate and identify potential WR binaries with compact-object companions.

The first such proposed object was WR 6 (a.k.a. HD 50896 or EZ CMa). Firmani et al. (1979, 1980) attributed the 3.7 d periodic variations in the emission line profiles to the interaction of the WR wind with a NS companion in an eccentric orbit. The variations were subsequently attributed to other phenomena, including two oppositely moving outflows (Matthews et al. 1991), an unspecified mechanism due to rotation (Drissen et al. 1989), periodic instabilities at the base of the wind (Flores et al. 2007), co-rotating interaction regions (CIRs; Ignace et al. 2013) and the interaction of the WR wind with a non-compact companion (Koenigsberger & Schmutz 2020). Despite nearly six decades of observational campaigns, there is as yet no theoretical radiative transfer study that is capable of reproducing the line profile variability that gave rise to these thus far speculative scenarios.

★ E-mail: j.toala@irya.unam.mx

Currently, only one candidate HMXB hosting a WR star and a BH was identified in the Galaxy (Cyg X-3; [van Kerkwijk et al. 1992](#)), and a few more in other galaxies ([Esposito et al. 2015](#)). The rarity of WR binaries with compact object became known as the problem of "missing WR X-ray binaries" (e.g., [van den Heuvel et al. 2017](#); [Vanbeveren et al. 2020](#)), though it has recently been argued that the majority of WR+compact-object binaries are not expected to be X-ray bright ([Sen et al. 2021](#)), a criticism that had been raised for WR 6, for example. Thus, it is therefore crucial to investigate whether other WR stars may be candidates for harbouring a compact object companion.

Variability has been used historically as a tool to search for and study the presence of companions ([Cherepashchuk & Khaliullin 1973](#); [Moffat & Shara 1986](#); [Koenigsberger & Schmutz 2020](#)) and has been further used to probe the wind properties in WR stars. As a consequence of the line-driven instabilities ([Castor et al. 1975](#); [Owocki et al. 1988](#)), winds from WR stars are not expected to be uniform. Inhomogeneities in their winds are expected to produce time-dependent fluctuations in the light curves, a type of variability also attributed at times to CIRs (see [St-Louis et al. 2009](#); [Cranmer and Owocki 1996](#)). Such structures are also thought to be responsible for linear polarization ([Robert et al. 1992](#); [Fullard et al. 2020](#)). Other mechanisms that have been proposed to cause wind variability are pulsations (see [Townsend 2007](#); [Grassitelli et al. 2016](#), and references therein). In fact, the connection between pulsations and outflowing wind structures has been demonstrated for at least one well-studied object, HD 64760 ([Kaufer et al. 2006](#)).

Among WR stars, those classified as part of the WN8 sequence are the most variable ([Antokhin et al. 1995](#); [Moffat & Shara 1986](#); [Marchenko et al. 1998](#)). Their low temperatures produce a (sub)surface convection zone due to the iron opacity bump ([Nugis & Lamers 2002](#); [Cantiello et al. 2009](#)), which may have consequences for their surface variability. On the other hand, early WN stars have stronger stellar winds and lower luminosities which make them less affected by the iron opacity bump ([Ro 2019](#)). As a consequence, one could expect that such stars are less prone to variability. However, variability has been also reported for early WN stars in the past decades (e.g., [Chené & St-Louis 2010](#); [Chené et al. 2011](#); [Marchenko et al. 1998](#); [Lamontagne 1983](#); [Koenigsberger et al. 1980](#); [Lenoir-Craig et al. 2022](#)). Recently, [Nazé et al. \(2021\)](#) showed that there is no apparent dichotomy in the variability between early and late WN stars.

In this paper we present the analysis of the optical variability from the WN4 star WR 7. Thus far, there are no suggestions of a companion reported in the literature. Radio observations searching for non-thermal emission as signatures of binary companions resulted only in upper limits for WR 7 ([Raguzova & Sidorenkov 2000](#)). Furthermore, there are no available UV or optical line variability studies of WR 7 that show the presence of CIRs. Recently, [Nazé et al. \(2021\)](#) presented the analysis of *Transit Exoplanet Survey Satellite* (*TESS*; [Ricker et al. 2015](#)) observations of a sample of WR and LBV stars, including WR 7. They analysed Sector 7 *TESS* observations of WR 7 and concluded that it exhibits coherent variability with a dominant period of 3.86 d^{-1} with some harmonic frequencies. Although they seem to suggest pulsations as the main physical mechanisms to explain such periodicity, [Nazé et al. \(2021\)](#) conclude that new pulsating models are needed to enhance our understanding of the observations.

In this paper we use *TESS* observations of WR 7 to corroborate multi-periodic variability of the order of days and hours. We complement these *TESS* data with high-resolution time-series spectroscopic observations to further study the variability of WR 7. In Section 2 we describe our observations and results are presented in Section 3. We

discuss the possible origins of the variability in Section 4. Finally, a summary is presented in Section 5.

2 OBSERVATIONS

The *TESS* satellite offers exciting and new opportunities to study the photometric variability of many massive stars to an unprecedented level of precision ([Bowman 2020](#)). In an initial search of variability in WR stars observed by *TESS*, we corroborated WR 7 as showing atypical properties. Specifically, its light curve and corresponding amplitude spectrum contains both long-period and significant short-period variability. The latter caught our attention and motivated us to seek out plausible mechanisms that may be responsible. *TESS* observed WR 7 during sector 7 (between 2019 Jan 8 and 2019 Feb 1) in the full-frame images (FFIs) with a 30-min cadence and during sectors 33 and 34 (between 2020 Dec 18 and 2021 Feb 8) both with a 2-min cadence and in the FFI with a 10-min cadence. We retrieved both 40×40 pixel cutouts from the FFIs with *ASTROCUT* ([Brasseur et al. 2019](#)), and short-cadence target pixel files (TPFs) from the Mikulski Archive for Space Telescopes (MAST)¹.

We found that because the short-cadence TPFs are much smaller than our own FFI pixel cutouts, their background flux estimates are non-negligibly contaminated by the nearby eclipsing binary OU CMa. Hence, we focus ourselves to the FFI data in this work and conclude that the light curves obtained from the SPOC pipeline applied to the 2-min TPF data are inferior. We estimated the background flux by taking the median observed flux per frame, excluding the pixels that predominantly contain stellar flux, and subtracted it from the measured flux values. The light curves were then obtained with custom-created aperture masks, normalised by dividing through the median flux and converted to units of mmag. Our FFI-extracted light curves from sectors 7, 33 and 34, together with the corresponding amplitude spectra, are shown in Fig. 1.

In addition to *TESS* data, we retrieved archival and recently acquired high-resolution spectroscopy for WR 7. The first set of spectra were secured with the Ultraviolet and Visual Echelle Spectrograph (UVES) instrument mounted on the UT2 of the Very Large Telescope (VLT). A total of 14 spectra were retrieved in reduced form from the European Southern Observatory (ESO) archive (program ID 080.D-0137, PI: Foellmi). The spectra were acquired back-to-back in the two nights of 2008 Jan 26–27 and have a nominal resolving power of $R \approx 30\,000$. We complemented these archival spectra with seven spectra acquired with the HERMES spectrograph ([Raskin et al. 2011](#)) mounted on the 1.2 m Mercator telescope in La Palma, Spain. These spectra have a nominal resolving power of $R \approx 80\,000$. The spectra were acquired in the framework of a long-term spectroscopic monitoring of Galactic WR stars (see [Dsilva et al. 2020](#), for details).

3 DATA ANALYSIS

3.1 *TESS* photometry

To assess the multiperiodic variability in the *TESS* light curves of WR 7, we used Fourier analysis to extract significant frequencies, amplitudes, phases and their respective uncertainties. As evidenced in Fig. 1, it became immediately apparent that the variability seen in WR 7 was different in sector 7 than in sectors 33 and 34, which implies a long term modulation to the variability given that these *TESS*

¹ <https://archive.stsci.edu/>

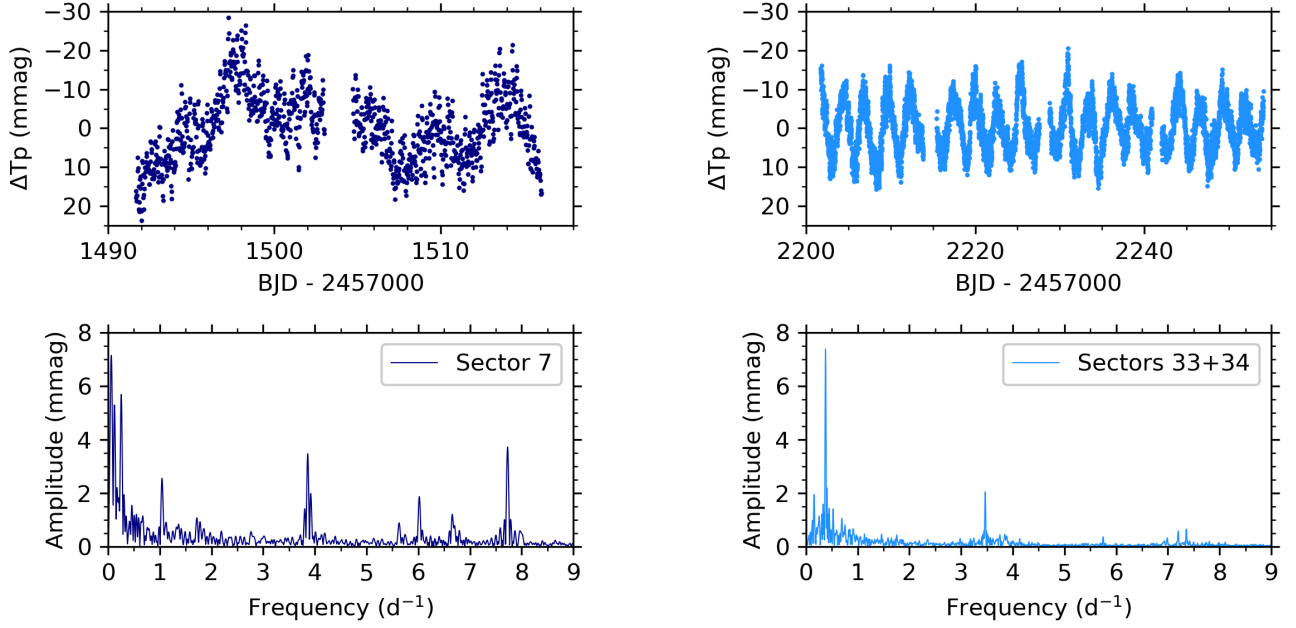


Figure 1. Background-subtracted *TESS* light curves of WR 7 (top panels) and their corresponding amplitude spectra (bottom panels) of our FFI data obtained in sector 7 (left) and sectors 33 and 34 combined (right). Long-term modulation is clearly detected in both the long- and short-period variability in WR 7.

sectors span almost 2 yr. Also, the *TESS* light curve from sector 7 is more noisy, which may be astrophysical given that WR variability is known to be dominated by stochastic signals associated with the clumpy aspherical winds in combination with stellar pulsations as suggested by Nazé et al. (2021). We employed the detrending methodology developed by Bowman et al. (2018) to the combined *TESS* sectors 33 and 34 light curve, since we deem it of higher quality for subsequent frequency analysis, to remove any remaining small instrumental trends. The detrended FFI light curve from sectors 33 and 34 is shown in the top-left panel of Fig. 2.

To determine the significant periodicities and their amplitudes in the *TESS* data, we fit sinusoids to the light curve using the PERIOD04 software (Lenz & Breger 2005), opting to treat the sector 7 light curve and the combined sectors 33 and 34 light curve separately. A significant frequency is defined as having an amplitude signal-to-noise ratio (SNR) larger than four following the empirical results of Breger et al. (1993). The noise is estimated using a local window of size 1 d^{-1} centred in the amplitude spectrum at the location of where a frequency has been removed during iterative pre-whitening. At the end of iterative pre-whitening and all significant ($\text{SNR} \geq 4$) frequencies have been extracted, we optimise their amplitudes, frequencies and phases using a cosinusoid function and a non-linear least-squares fit to the light curve (see, e.g., Bowman & Michielsen 2021). In total we find eight significant frequencies in the sector 7 light curve and a different eight significant frequencies in the combined sectors 33 and 34 light curve, which range between approximately 0.3 and 8.0 d^{-1} , and have amplitudes up to 7.45 mmag . A complete list of significant frequencies, including their optimised amplitudes, phases and corresponding uncertainties from the sector 7 and combined light curve from sectors 33 and 34, is given in Table 1.

Similarly to what is reported in Nazé et al. (2021) for sector 7, we found that the highest amplitude feature corresponds to a frequency of $7.728 \pm 0.002 \text{ d}^{-1}$, but this is very likely a harmonic of the $3.862 \pm 0.003 \text{ d}^{-1}$ frequency. That is, a dominant period of

Table 1. Frequencies, amplitudes and phases of the significant (i.e. $\text{SNR} \geq 4$) signals in the *TESS* photometry of WR 7. Because of the long-term amplitude and frequency modulation in WR 7, the sector 7 and sectors 33 and 34 data are analysed separately. 1σ uncertainties are calculated from the multi-frequency non-linear least-squares fit, using the phase zero-points of BJD 2458505.0 and BJD 2459225.0, respectively.

Frequency (d^{-1})	Amplitude (mmag)	Phase (rad)
Sector 7		
1.04378 ± 0.00283	2.54 ± 0.33	-2.39 ± 0.13
3.86187 ± 0.00265	3.17 ± 0.33	2.73 ± 0.11
3.92136 ± 0.00734	1.14 ± 0.33	-0.61 ± 0.31
5.62808 ± 0.00923	0.78 ± 0.33	1.18 ± 0.43
6.02026 ± 0.00396	1.83 ± 0.33	1.46 ± 0.18
6.65874 ± 0.00628	1.15 ± 0.33	3.03 ± 0.29
7.72781 ± 0.00198	3.68 ± 0.33	3.06 ± 0.09
7.98967 ± 0.01404	0.52 ± 0.33	2.03 ± 0.65
Sectors 33 and 34		
0.37832 ± 0.00007	7.45 ± 0.05	2.03 ± 0.01
0.75424 ± 0.00070	0.76 ± 0.05	2.68 ± 0.07
1.12990 ± 0.00136	0.39 ± 0.05	-2.85 ± 0.13
3.46785 ± 0.00026	2.02 ± 0.05	-0.92 ± 0.03
5.74754 ± 0.00144	0.37 ± 0.05	2.56 ± 0.14
6.99000 ± 0.00190	0.28 ± 0.05	0.98 ± 0.19
7.20050 ± 0.00087	0.62 ± 0.05	0.81 ± 0.09
7.35643 ± 0.00079	0.68 ± 0.05	-2.15 ± 0.08

$0.25894 \pm 0.0002 \text{ d}$ ($\approx 6.22 \text{ h}$). However, the longer time base, larger number of data points, and improved noise statistics of the combined sectors 33 and 34 light curve provides better precision on the resultant frequencies compared to those of sector 7. In the combined sectors 33 and 34 light curve, the dominant variability has a frequency of $0.37832 \pm 0.00007 \text{ d}^{-1}$, that is, a period of $2.6433 \pm 0.0005 \text{ d}$. Other

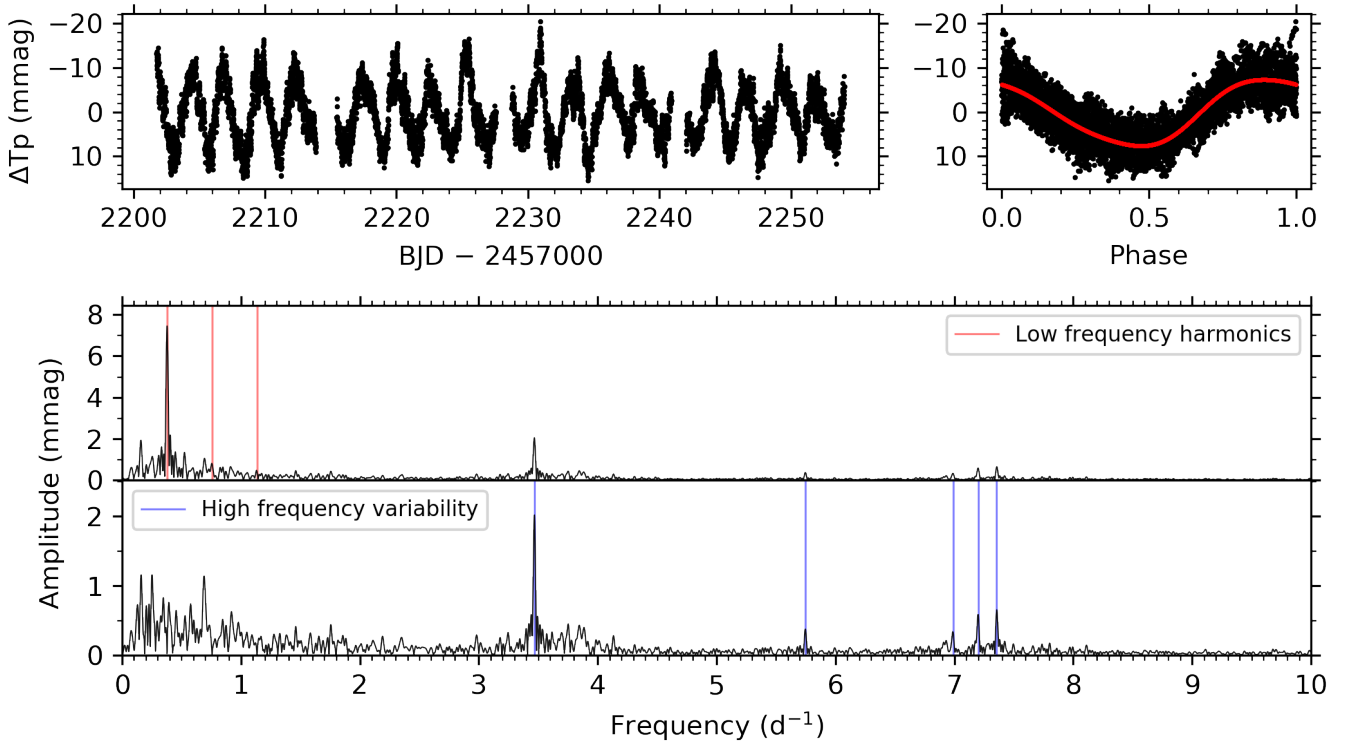


Figure 2. Detrended 10-min FFI *TESS* light curve of WR 7 from sectors 33 and 34 (upper left panel), the phase-folded light curve (upper right panel) for the dominant period of 2.6433 d, the amplitude spectrum (middle panel) and residual amplitude spectrum (bottom panel) after subtracting the dominant frequency and two significant harmonics, which are shown as vertical red lines. Vertical blue lines represent significant short period variability (cf. Table 1).

significant frequencies include harmonics of this period (see Table 1). The phase-folded light curve from sectors 33 and 34 based on this dominant period and its two significant harmonics is shown in the top-right panel of Fig. 2. In the bottom panel, the original and residual amplitude spectra (i.e. after subtracting the dominant period and its two significant harmonics) are shown. The presence of harmonics indicate the non-sinusoidal nature of the long-period variability, and suggest rotation modulation or binarity as possible causes. The vertical blue lines in the bottom panel of Fig. 2 denote the location of the significant high frequency variability in the amplitude spectrum.

In general, we detect high-amplitude, high-frequency variability with frequencies between 3–10 d^{-1} that appear in both *TESS* sector observations of WR 7 which were previously inferred to be associated with stellar pulsations (Nazé et al. 2021). Nevertheless, the amplitudes and frequencies between sector 7 and those of sectors 33 and 34 light curves are significantly different (see Table 1 and Fig. 1). Not only do the amplitude and frequencies of the short-period variability change significantly, the dominant period of the 33+34 sector (2.64 d) is not detectable in the sector 7 data. This clearly demonstrates that WR 7 has multiple variability time-scales of order days and hours, respectively, which are both modulated on the time scale of years given the gap of ~ 2 yr between the sectors 7 and the sectors 33 and 34 light curves. Such an apparent incoherence and clear modulation of both long- and short-period variability in a WR is intriguing and points to an astrophysical explanation. We note that epoch-dependent measurements have also been reported by Lenoir-Craig et al. (2022) for other galactic WR stars. Hence, such variability is difficult to reconcile as coherent pulsations given its long-term modulation of order months-to-years. On the other hand, coherent pulsations in the

photosphere of a WR star would be heavily obscured and strongly modulated by the clumpy wind.

Moreover, we investigated if the variability seen in the *TESS* data of WR 7 could be caused by contamination, and confirmed that the observed variability is intrinsic to WR 7. Aside from small-scale variations depending on the chosen aperture mask, the level of flux contamination in the final light curve is only ~ 5 per cent. In addition, the observed amplitude of the short-period variability is maximal at the location of WR 7 on the CCD and correlates with the flux contribution of WR 7 within a given pixel of the CCD, providing strong support for the variability originating in WR 7. This is assuming, however, that WR 7 does not have an as-of-yet detected binary companion.

3.2 Spectroscopy

To further investigate the origin of the periods identified in the *TESS* light curves, we show a residual dynamical spectrum of WR 7 using the UVES data and focusing on the N v $\lambda\lambda 4604, 4620$ doublet and the H β region in Fig. 3. Since the UVES spectra are of much higher SNR than the HERMES spectra and were taken on a short cadence (see Fig. 3), we refrain from combining them with the HERMES data. The residual spectra were formed by computing the difference between each spectrum and the mean spectrum, plotted below the dynamical spectra for reference.

The dynamical spectra reveal structures in both these line complexes. The H β line shows strips of emission or absorption propagating in Doppler space with time from the line centre. The H β line profile displays narrow emission peaks that travel from near the line centre out to $\gtrsim 1000$ $km\ s^{-1}$ in ~ 0.25 d during two consecutive

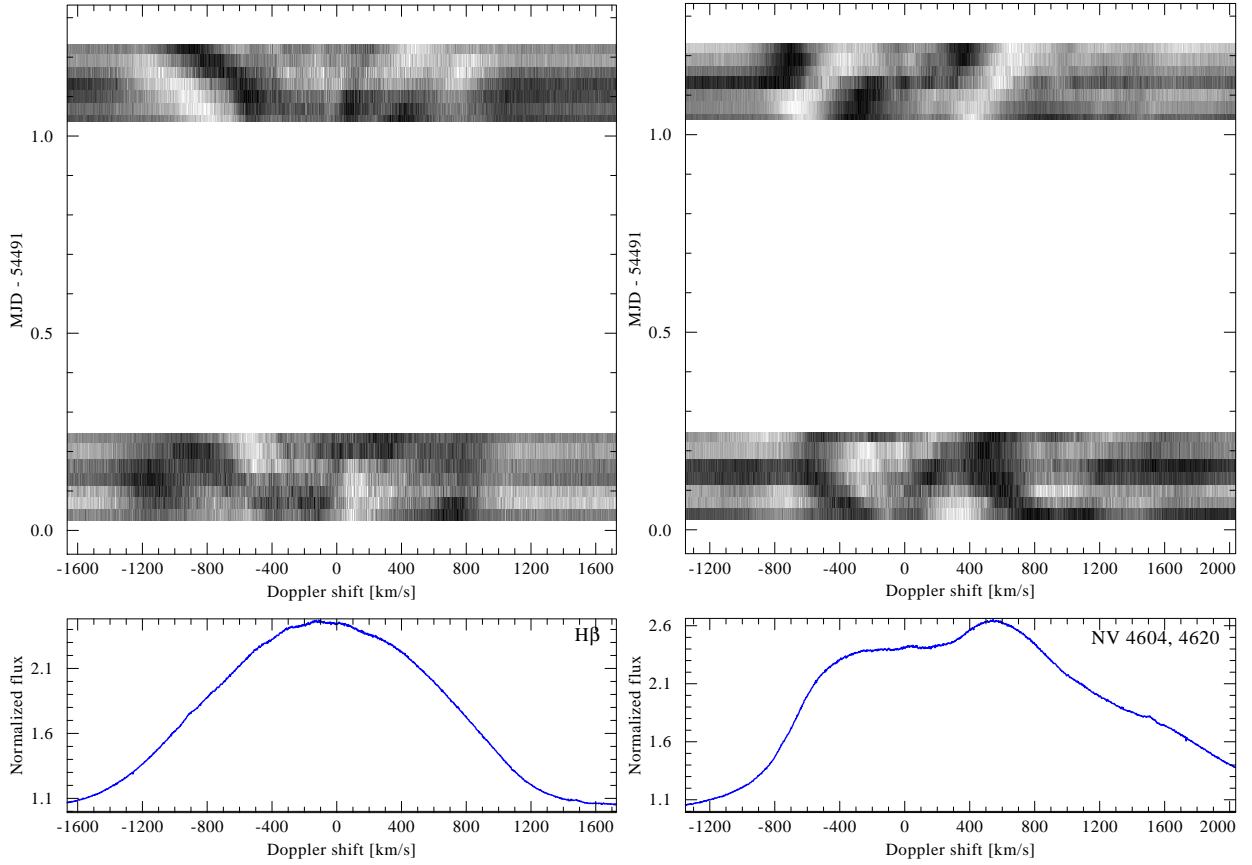


Figure 3. Residual dynamical spectra for the UVES data, zooming on the $H\beta$ (left) and the $N\text{v } \lambda\lambda 4604, 4620$ doublet region (right) lines. The panels below each dynamical spectrum show the mean spectrum subtracted from each observation.

nights. Such a pattern is typically associated with clumps propagating outwards in the stellar wind (Lépine & Moffat 1999). On the other hand, the $N\text{v}$ seems to suggest a more peculiar variability. It shows preferentially negative-velocity moving peaks during the first night and positive-velocity peaks on the second night. The latter resembles CIR-like variability, as seen for example in WR 1 (Chené & St-Louis 2010) or could be a manifestation of mass transfer (Packet 1981) to an unseen companion.

We attempted to phase-fold the spectra with the main periods found in the *TESS* data. However, none of these attempts resulted in coherent dynamical spectra. Notably, we cannot identify the strong 2.64 d signal obtained from the *TESS* data analysis in the UVES data. While we cannot determine a period from the available spectroscopic data, an inspection of the apparent CIR patterns in the $N\text{v } \lambda\lambda 4604, 4620$ doublet (Fig. 3) suggests a possible periodicity of the order of 0.4 d. However, continuous time coverage along a few cycles is needed to verify this.

To investigate the possible binary hypothesis of WR 7 motivated by the presence of unexpected high-frequency variability indicative of pulsation modes in the *TESS* data, we measured the radial velocities (RVs) of WR 7 using both the UVES and HERMES data sets (Dsilva et al. 2020, Dsilva et al. submitted to A&A). The measurements rely on the method of cross-correlation of the $N\text{v } \lambda 4945$ line with a template constructed by co-adding all observations iteratively (see Zucker 2003; Shenar et al. 2019; Dsilva et al. 2020, for details). The $N\text{v } \lambda 4945$ emission line is chosen since it exhibits the least amount of variability of all available lines. The RVs are relative, as they are measured with respect to a co-added template with arbitrary

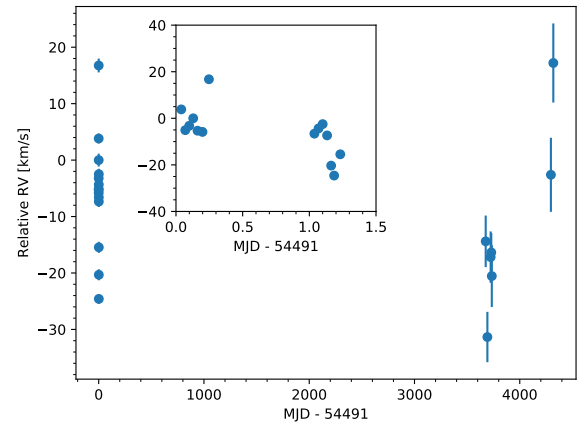


Figure 4. RVs of the $N\text{v } \lambda 4945$ line in the available UVES and HERMES spectra. The inset shows the details of the earliest observations.

calibration. It is important to note that the measured RVs may be impacted by substantial spectral variability.

The RVs of the $N\text{v } \lambda 4945$ line, covering roughly 10 years, are shown in Fig. 4. We tried to phase-fold the RVs with either $P = 2.64$ d or $P = 0.288$ d (the second most intense feature in the *TESS* amplitude spectrum of WR 7), but no noticeable pattern emerged. While substantial RV variability is seen, its erratic nature suggests that it originates in line-profile variability rather than Doppler shifts. Moreover, no clear long-term systematic shift is observed. Hence,

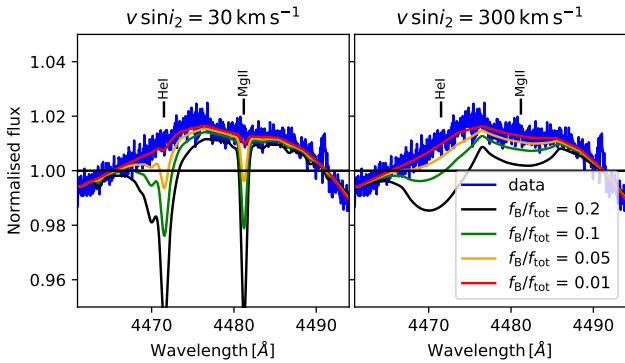


Figure 5. The two panels show the co-added UVES spectrum of WR 7, focusing on the He I $\lambda 4471$ and Mg II $\lambda 4482$ lines. Also shown are combinations of a WR template and a B-star template, representing a putative B-type companion, with varying light contributions (see legend). For the B-type spectrum, we use a TLUSTY model atmosphere of a late B-type star ($T_{\text{eff}} = 15$ kK, $\log g = 4.0$ [cgs]). For the WR template, we do not use model atmospheres since they generally do not reproduce the underlying profile to the needed level of accuracy. Instead, we use the spectrum itself, binned at 4 \AA . We show this for a slow rotator ($v \sin i_2 = 30 \text{ km s}^{-1}$, left panel) and a rapid rotator ($v \sin i_2 = 300 \text{ km s}^{-1}$, right panel).

while a companion cannot be ruled out from the RV measurements, no clear evidence for a companion is seen from the RV variability.

In an attempt to constrain the presence of a possible non-degenerate stellar companion in WR 7, we furthermore critically inspect the co-added UVES spectrum ($\text{SNR} \approx 500$) and compare it with synthetic OB-type model spectra obtained from publicly available grids calculated with the TLUSTY model atmosphere code (Hubeny & Lanz 1995; Lanz and Hubeny 2007). Since a companion is not readily apparent in the co-added spectrum or the RV variability, it is clear that a putative companion cannot be of earlier spectral type (see examples in Shenar et al. 2019). We therefore consider companions in the range $T_{\text{eff}} \lesssim 30$ kK. In this regime, aside from the Balmer lines, which would be heavily entangled with the WR emission lines, the strongest lines are He I $\lambda 4471$ and Mg II $\lambda 4482$, where the latter becomes stronger as the temperature drops. As an example, Fig. 5 shows the impact a late-type B star would have on the spectrum for various light ratios, and considering a slow and a rapid rotator. The light ratio and the projected rotational velocity are the two limiting factors here. As Fig. 5 illustrates, we can rule out companions contributing as little as $\approx 2\text{--}3\%$ if slow rotation is assumed, which goes up to $\approx 5\text{--}10\%$ if rapid rotation is assumed.

To translate these limits into rough spectral type thresholds, we use calibrations between spectral types and visual magnitudes by Schmidt-Kaler (1982). Given the evident faintness of a potential companion, we attribute the derived absolute visual magnitude of $M_V = -3.62$ mag (Hamann et al. 2019) to WR 7. Our thresholds therefore correspond to maximum magnitudes of $M_{V,2} \approx 0.6$ mag for the slow rotator case and $M_{V,2} \approx -1.1$ mag for the rapid rotator case. These threshold magnitudes correspond roughly to A0 V and B5 V, respectively. We note that the very shallow and broad absorption features seen in Fig. 5, which have a depth of the order of the SNR, could be interpreted as photospheric absorption. However, their presence sensitively depends on the normalisation of the data.

Thus, we can rule out companions earlier than about B5 V. A late-type rapidly rotating B-type companion cannot be ruled out with this analysis. A-type companions are difficult to imagine, given that the timescale for their formation from the pre-main-sequence

star approaches or exceeds the timescale for forming a WR star. Another alternative is that WR 7 hosts a compact object (WR+cc). As discussed by Toalá et al. (2018) for the case of WR 124, WR+cc systems are not necessarily X-ray bright. A NS would easily escape detection through our RV monitoring, given the spectral variability (cf. Fig. 4).

4 DISCUSSION

The optical data presented in this work unambiguously show that WR 7 exhibits a range of variability time scales. The analysis of multi-instrument observations confirms that WR 7 has variability time scales of the order of days and hours, which are also modulated in scale of years. Variability in WR stars might be caused by different factors involving companions, pulsations and density structures in their winds. In the following we assess these possibilities as the cause of the observed small frequencies ($< 3 \text{ d}^{-1}$) detected from WR 7, in particular, that corresponding to a period of 2.64 d. We note that, as discussed by Nazé et al. (2021), the variability periods between 3 and 10 d^{-1} may be pulsations if they do not originate from a companion.

The relatively longer period of the dominant variability (~ 2.64 d) obtained from sectors 33+34 of the *TESS* data is difficult to reconcile as pulsations (see, e.g., Scuflaire & Noels 1986; Glatzel & Mehren 1996). Theoretical work by Grassitelli et al. (2016) who used numerical calculations of pulsating WR stars with masses around $M_\star = 9\text{--}15 M_\odot$ (covering the mass range of WR 7) found that their pulsation periods are of the order of minutes. This is a much shorter-period regime than any of the observed frequencies in the *TESS* light curve. Thus, we discard pulsations from WR 7 as the source of dominant variability ($P = 2.64$ d) in sectors 33+34. In contrast, we note that the 9.8 h period variability detected from WR 123 (Lefèvre et al. 2005) has been reproduced by radiation-hydrodynamic simulations of pulsations of massive hydrogen-rich stellar envelopes of stars in the $22\text{--}27 M_\odot$ range presented by Dorfi et al. (2006) (see also the work of Glatzel 2008; Townsend & MacDonald 2006).

A large fraction of WR stars have been reported to be part of binary systems with stellar or compact companions². van der Hucht (2001) list that about 40 per cent of WR stars host binary companions. However, we note that such percentage could be higher if WR stars are part of long-period systems (see Dsilva et al. 2020). Thus, it would not be unusual to find that WR 7 is also in a binary system.

According to our spectroscopic analysis, a binary companion earlier than B5 V can be ruled out, but not a rapidly-rotating B-type star. Thus, an example candidate in this restricted mass range is a Be star. These objects are accepted to be rapidly rotating main sequence B stars that exhibit variability due to non-radial pulsation modes with periods between 0.01 and 10 d (see, e.g., Table 1 in Rivinius et al. 2013). Recently, Labadie-Bartz et al. (2020) used *TESS* observations of more than 400 classical Be stars to show that they exhibit multiperiodic variability in the frequency regime between about $0.25\text{--}4 \text{ d}^{-1}$, but can be higher in Be stars rotating near their critical break-up velocity. Nevertheless, we note that a unique characteristic of Be stars is the presence of an decretion disk, usually detected through Balmer lines in emission (Rivinius et al. 2013), which we do not see from the WR 7 spectroscopic data.

There is now a large number of binary systems that have been shown to display tidally-excited oscillations (TEOs) on a wide variety of timescales (see, e.g., Welsh et al. 2011; Fuller & Lai 2012; Guo

² See the P. Crowther WR Star Catalogue (Rosslowe & Crowther 2015) <http://pacrowther.staff.shef.ac.uk/WRcat/index.php>

et al. 2017; Guo 2020, and references therein). If WR 7 possesses a binary companion and the orbit were even slightly eccentric, TEOs may be excited in one of the stars. Depending on their relative brightness and the pulsation amplitudes, either one or both sets of TEOs might be detectable. Furthermore, given the connection that has been shown to exist between pulsations and the formation of a structured wind (Kaufer et al. 2006; Townsend 2007), the WN TEO pulsations would naturally give rise to the sub-features that are observed in its emission lines. WR 7 would not be the first WR system in which TEOs are discovered, given recent *TESS* results on the SMC system HD 5980 (Kołaczek-Szymański et al. 2021). But we emphasise that this hypothesis is purely speculative given the unclear binary status of WR 7.

To further peer into the possible binary status of WR 7, we re-analyzed the available *XMM-Newton* EPIC data. We confirmed that the X-ray emission from WR 7 is soft (Zhekov 2014; Toalá et al. 2015) and consistent with the self-shocking wind mechanism in WR stars (Oskinova 2015). We created multi-band light curves and found no signs of variability. Unfortunately, the lack of variability in X-rays can not rule out the presence of compact companions (Sen et al. 2021; Toalá et al. 2018).

Other than WR 7, there is only one case reported to exhibit low-frequency quasi-coherent variability, namely WR 134. A period of 2.3 d has been reported in the past decades by several authors, suggesting that its signal is long lived (Morel et al. 1999; McCandless et al. 1994; Nazé et al. 2021). On the other hand, the dominant period of 2.64 d obtained from sectors 33+34 is not detected in sector 7 observations. Even though the sector 7 data are noisy, on average, the non-detection of the same period appears to be a robust result.

The analysis of the *TESS* data of WR 7 presented here suggests a non-sinusoidal nature for the dominant variability, which is typically the signature of rotational modulation. This is suggestive of the presence of a CIR in the wind (see, e.g., the case of WR 110; Chené et al. 2011) and, if this is the case, the real period of the variability would be 2×2.64 d (~ 5.3 d), given that CIR are usually present in pairs. Adopting a stellar radius of $1.26 R_{\odot}$ (see Hamann et al. 2019), we estimate a rotation velocity of 12.0 km s^{-1} for WR 7, which is too small to be detectable via rotational line broadening (see Shenar et al. 2014).

We conclude that given the lack of strong evidence from a binary companion in the currently available data, WR 7 seemingly pulsates in quasi-coherent modes in addition to variability caused by CIRs on top of a background of stochastic low-frequency variability (see, e.g., Bowman et al. 2019; Nazé et al. 2021). If the high-frequency variability does originate in WR 7 and is caused by pulsations, such a result represents an interesting challenge to our current understanding of the rotational, wind and pulsational properties of WR stars (Nazé et al. 2021).

5 CONCLUSIONS

We presented the analysis of multi-instrument optical observations of the early WN-type star WR 7. *TESS* data were used to unveil the presence of a dominant variability with a period of 2.6433 ± 0.0005 d in addition to previously-reported high-frequency features with frequencies between $3\text{--}10 \text{ d}^{-1}$, which have been recently attributed to stellar pulsations (Nazé et al. 2021).

Using high-resolution spectroscopic observations from VLT UVES we detect small scale variations in the wind of WR 7. The dynamical spectra of the $H\beta$ line suggest the presence of radially-expanding clumps in the wind of WR 7, but that of the $N\text{v}$ suggest

negative-velocity moving peaks during the first night and positive-velocity peaks on the second night. This could be the manifestation of mass transfer to an unseen companion or a large scale outflow emerging from only one hemisphere of a rotating star. The UVES observations are further used in combination with TLUSTY stellar atmosphere models to reject the presence of a companion as late as A0 V in the case of a slow rotator and a B5 V for a rapid rotator case. RVs measured for the WR component using the UVES data and additional HERMES data across a 10 yr baseline are variable, with a peak-to-peak amplitude of $\Delta RV \approx 50 \text{ km s}^{-1}$, but do not give clear indication for orbital Doppler motion in WR 7.

Several mechanisms producing the dominant period in the *TESS* data of sectors 33+34 of WR 7 are explored. There are no strong indicators of the presence of a companion, even a compact object might be difficult to unveil (Sen et al. 2021; Toalá et al. 2018). A period of 2.64 d is difficult to reconcile with theoretical predictions from stellar pulsation models (Grassitelli et al. 2016).

By exploring the presence of CIRs in the wind as possibility, the real period is estimated to be ≈ 5.3 d. If this is the case, we estimate a rotation velocity of 12 km s^{-1} for WR 7, which would be undetected given the line broadening because of the much faster wind velocities of this WR star.

WR 7 exhibits multi-period variability with time scales of the order of days and hours, which are also modulated on time scales of years. Although the presence of a stellar or compact companion cannot be rejected, it seems that a variety of phenomena is taking place in WR 7. This early N-rich WR star seems to pulsate in quasi-coherent modes in addition to variability caused by slow CIRs that might have been overlooked in previous stellar atmosphere analysis, in addition to stochastic low-frequency variability. WR 7 seems to be pushing forward our understanding of variability in evolved massive stars. High-resolution, continuous monitoring of this star, in addition to the most updated radiation-hydrodynamic simulations of winds from WR stars (see, e.g., Moens et al. 2022), is needed in order to unveil the physics behind the observed multiple variability time scales.

ACKNOWLEDGEMENTS

We would like to thank the anonymous referee for a detailed review on our manuscript which improved the presentation of our analysis. JAT acknowledges funding by DGAPA UNAM PAPIIT project IA101622 and the Marcos Moshinsky Foundation (Mexico). DMB and TVR gratefully acknowledge senior and junior postdoctoral fellowships from the Research Foundation Flanders (FWO) with grant agreement numbers 1286521N and 12ZB620N, respectively. KS and TS acknowledge funding received from the European Research Council (ERC) under the European Union’s Horizon 2020 research and innovation programme (grant agreement number 772225: MULTIPLES). TS further acknowledges support from the European Union’s Horizon 2020 under the Marie Skłodowska-Curie grant agreement No 101024605. GK acknowledges support from CONACYT grant 252499 and DGAPA UNAM PAPIIT grant IN103619.

The *TESS* data presented in this paper were obtained from the Mikulski Archive for Space Telescopes (MAST) at the Space Telescope Science Institute (STScI), which is operated by the Association of Universities for Research in Astronomy, Inc., under NASA contract NAS5-26555. Support to MAST for these data are provided by the NASA Office of Space Science via grant NAG5-7584 and by other grants and contracts. Funding for the *TESS* mission was provided by the NASA Explorer Program. This research has made

use of the SIMBAD database, operated at CDS, Strasbourg, France; the SAO/NASA Astrophysics Data System; and the VizieR catalog access tool, CDS, Strasbourg, France.

DATA AVAILABILITY

The data underlying this article will be shared on reasonable request to the corresponding author.

REFERENCES

- Abbott, B. P., Abbott, R., Abbott, T. D., et al. 2019, *Physical Review X*, 9, 031040. doi:10.1103/PhysRevX.9.031040
- Antokhin, I., Bertrand, J.-F., Lamontagne, R., et al. 1995, *AJ*, 109, 817
- Bowman, D. M., Buyschaert, B., Neiner, C., et al. 2018, *A&A*, 616, A77
- Bowman, D. M., Aerts, C., Johnston, C., et al. 2019, *A&A*, 621, A135
- Bowman, D. M., Michielsen, M., 2021, *A&A*, 656, A158
- Bowman, D. M. 2020, *Frontiers in Astronomy and Space Sciences*, 7
- Brasseur, C. E., Phillip, C., Fleming, S. W., et al. 2019, *Astrocute: Tools for creating cutouts of TESS images*, ascl:1905.007.
- Breger, M., Stich, J., Garrido, R., et al. 1993, *A&A*, 271, 482.
- Brott, I., Evans, C. J., Hunter, I., et al. 2011, *A&A*, 530, A116
- Cantiello, M., Langer, N., Brott, I., et al. 2009, *A&A*, 499, 279.
- Castor, J. I., Abbott, D. C., & Klein, R. I. 1975, *ApJ*, 195, 157
- Chené, A.-N., Foellmi, C., Marchenko, S. V., et al. 2011, *A&A*, 530, A151
- Chené, A.-N. & Moffat, A. F. J. 2011, *Active OB Stars: Structure, Evolution, Mass Loss, and Critical Limits*, 272, 445
- Chené, A.-N. & St-Louis, N. 2010, *ApJ*, 716, 929
- Cherepashchuk, A. M. & Khaliullin, K. F. 1973, *Soviet Ast.*, 17, 330
- Conti, P. S. 1975, *Memoires of the Societe Royale des Sciences de Liege*, 9, 193
- Cranmer, S. R., Owocki, S. P. 1996, *ApJ*, 462, 469 doi:10.1086/177166
- Crowther, P. A. 2007, *ARA&A*, 45, 177
- de Mink, S. E., Langer, N., Izzard, R. G., et al. 2013, *ApJ*, 764, 166. doi:10.1088/0004-637X/764/2/166
- Dorfi, E. A., Gautschi, A., & Saio, H. 2006, *A&A*, 453, L35. doi:10.1051/0004-6361/200600027
- Drissen, L., Robert, C., Lamontagne, R., et al. 1989, *ApJ*, 343, 426
- Dsilva, K., Shenar, T., Sana, H., et al. 2020, *A&A*, 641, A26
- Esposito, P., Israel, G. L., Milisavljevic, D., et al. 2015, *MNRAS*, 452, 1112
- Firmani, C., Koenigsberger, G., Bisiacchi, G. F., et al. 1980, *ApJ*, 239, 607
- Firmani, C., Koenigsberger, G., Bisiacchi, G. F., et al. 1979, *Mass Loss and Evolution of O-Type Stars*, 83, 421
- Flores, A., Koenigsberger, G., Cardona, O., et al. 2007, *AJ*, 133, 2859
- Foellmi, C., Moffat, A. F. J. et al. 2003, *MNRAS*, 338, 1025
- Fullard, A. G., St-Louis, N., Moffat, A. F. J., et al. 2020, *AJ*, 159, 214
- Fuller, J. & Lai, D. 2012, *MNRAS*, 420, 3126
- Glatzel, W. & Mehren, S. 1996, *MNRAS*, 282, 1470. doi:10.1093/mnras/282.4.1470
- Glatzel, W. 2008, *Hydrogen-Deficient Stars*, 391, 307
- Grassitelli, L., Chené, A.-N., Sanyal, D., et al. 2016, *A&A*, 590, A12
- Guo, Z. 2020, *Stars and their Variability Observed from Space*, 203
- Guo, Z., Gies, D. R., & Fuller, J. 2017, *ApJ*, 834, 59
- Hainich, R., Ramachandran, V., Shenar, T., et al. 2019, *A&A*, 621, A85. doi:10.1051/0004-6361/201833787
- Hainich, R., Pasemann, D., Todt, H., et al. 2015, *A&A*, 581, A21. doi:10.1051/0004-6361/201526241
- Hamann, W.-R., Gräfener, G., Liermann, A., et al. 2019, *A&A*, 625, A57
- Hamann, W.-R., Gräfener, G., & Liermann, A. 2006, *A&A*, 457, 1015
- Hubeny I., Lanz T., 1995, *ApJ*, 439, 875. doi:10.1086/175226
- Hubrig S., Scholz K., Hamann W.-R., Schöller M., Ignace R., Ilyin I., Gayley K. G., et al., 2016, *MNRAS*, 458, 3381. doi:10.1093/mnras/stw558
- Humphreys, R. M. 2010, *Hot and Cool: Bridging Gaps in Massive Star Evolution*, 425, 247
- Ignace, R., Gayley, K. G., Hamann, W.-R., et al. 2013, *ApJ*, 775, 29
- Kaufer, A., Stahl, O., Prinja, R. K., et al. 2006, *A&A*, 447, 325
- Kolaczek-Szymański, P. A., Pigulski, A., Michalska, G., et al. 2021, *A&A*, 647, A12
- Koenigsberger, G. & Schmutz, W. 2020, *A&A*, 639, A18
- Koenigsberger, G., Firmani, C., & Bisiacchi, G. F. 1980, *Rev. Mex. Astron. Astrofis.*, 5, 45
- Matthews, J. M., St. Louis, N., Drissen, L., et al. 1991, *J. R. Astron. Soc. Canada*, 85, 214
- Neugent, K. F. & Massey, P. 2014, *ApJ*, 789, 10. doi:10.1088/0004-637X/789/1/10
- Labadie-Bartz, J., Carciofi, A. C., de Amorim, T. H., et al. 2020, *arXiv:2010.13905*
- Lamontagne, R. 1983, Ph.D. thesis, Université de Montréal.
- Lanz, T. and Hubeny, I.: 2007, *The Astrophysical Journal Supplement Series* 169, 83. doi:10.1086/511270.
- Lefèvre, L., Marchenko, S. V., Moffat, A. F. J., et al. 2005, *ApJ*, 634, L109
- Lenoir-Craig, G., St-Louis, N., Moffat, A. F. J., et al. 2022, *ApJ*, 925, 79
- Lépine, S. & Moffat, A. F. J. 1999, *ApJ*, 514, 909. doi:10.1086/306958
- Lenz, P., Breger, M., 2005, *Comm. Asteroseismology*, 146, 53-136.
- McCandliss, S. R., Bohannon, B., Robert, C., et al. 1994, *Ap&SS*, 221, 155. doi:10.1007/BF01091149
- Marchenko, S. V., Moffat, A. F. J., van der Hucht, K. A., et al. 1998, *A&A*, 331, 1022
- Moens, N., Poniatowski, L. G., Hennicker, L., et al. 2022, *arXiv:2203.01108*
- Moffat, A. F. J., Marchenko, S. V., Zhilyaev, B. E., et al. 2008, *ApJ*, 679, L45
- Moffat, A. F. J., Drissen, L., Lamontagne, R., et al. 1988, *ApJ*, 334, 1038
- Moffat, A. F. J. & Shara, M. M. 1986, *AJ*, 92, 952
- Morel, T., Marchenko, S. V., Eenens, P. R. J., et al. 1999, *ApJ*, 518, 428. doi:10.1086/307250
- Mullan, D. J. 1984, *ApJ*, 283, 303. doi:10.1086/162307
- Nazé, Y., Rauw, G., & Gosset, E. 2021, *MNRAS*, 502, 5038. doi:10.1093/mnras/stab133
- Nugis, T. & Lamers, H. J. G. L. M. 2002, *A&A*, 389, 162
- Oskinova, L. M. 2015, *Wolf-Rayet Stars*, 295
- Owocki, S. P., Castor, J. I., & Rybicki, G. B. 1988, *ApJ*, 335, 914
- Packet, W. 1981, *A&A*, 102, 17
- Paczyński, B. 1967, *Acta Astron.*, 17, 355
- Raguzova, N. V. & Sidorenkov, V. N. 2000, *A&A*, 354, 551
- Ramiramantsoa, T., Ignace, R., Moffat, A. F. J., et al. 2019, *MNRAS*, 490, 5921
- Raskin, G., van Winckel, H., et al. 2011, *A&A*, 526, 6
- Rauw, G., Gosset, E., Manfroid, J., et al. 1996, *A&A*, 306, 783
- Ricker, G. R., Winn, J. N., Vanderspek, R., et al. 2015, *Journal of Astronomical Telescopes, Instruments, and Systems*, 1, 014003
- Rivinius, T., Carciofi, A. C., & Martayan, C. 2013, *A&ARv*, 21, 69
- Ro, S. 2019, *ApJ*, 873, 76
- Robert, C., Moffat, A. F. J., Drissen, L., et al. 1992, *ApJ*, 397, 277
- Rosslowe, C. K. & Crowther, P. A. 2015, *MNRAS*, 447, 2322
- Rustamov, D. N. & Cherepashchuk, A. M. 2012, *Astronomy Reports*, 56, 761
- Rustamov, D. N. & Cherepashchuk, A. M. 2011, *Astronomy Reports*, 55, 347
- Sana, H., de Mink, S. E., de Koter, A., et al. 2012, *Science*, 337, 444
- Scuflaire, R. & Noels, A. 1986, *A&A*, 169, 185
- Sen, K., Xu, X.-T., Langer, N., et al. 2021, *A&A*, 652, A138
- Schmidt-Kaler 1982, *Landolt-Börnstein VI*, 2, 17
- Shenar, T., Hamann, W.-R., Todt, H. 2014, *A&A*, 562, A118
- Shenar, T., Hainich, R., Todt, H., et al. 2016, *A&A*, 591, A22
- Shenar, T., Sablowski, D. P., Hainich, R., et al. 2019, *A&A*, 627, A151. doi:10.1051/0004-6361/201935684
- Shenar, T., Gilks, A., et al. 2020, *A&A*, 634, 79
- Sota, A., Maíz Apellániz, J., Morrell, N. I., et al. 2014, *ApJS*, 211, 10
- St-Louis, N., Chené, A.-N., Schnurr, O., et al. 2009, *ApJ*, 698, 1951
- Toalá, J. A., Oskinova, L. M., Hamann, W.-R., et al. 2018, *ApJ*, 869, L11
- Toalá, J. A., Guerrero, M. A., Chu, Y.-H., et al. 2015, *MNRAS*, 446, 1083
- Townsend, R. 2007, *Unsolved Problems in Stellar Physics: A Conference in Honor of Douglas Gough*, 948, 345
- Townsend, R. H. D. & MacDonald, J. 2006, *MNRAS*, 368, L57. doi:10.1111/j.1745-3933.2006.00157.x
- van der Hucht, K. A. 2001, *New Astron. Rev.*, 45, 135

- van Kerkwijk, M. H., Charles, P. A., Geballe, T. R., et al. 1992, *Nature*, 355, 703
- Vanbeveren, D. De Donder, E. et al. 1998, *New Astron.*, 3, 443
- Vanbeveren, D., Mennekens, N., van den Heuvel, E. P. J., et al. 2020, *A&A*, 636, A99. doi:10.1051/0004-6361/201937253
- van den Heuvel, E. P. J., Portegies Zwart, S. F., and de Mink, S. E., 2017, *MNRAS*, 471, 4256
- Weis, K. 2001, *Reviews in Modern Astronomy*, 14, 261
- Welsh, W. F., Orosz, J. A., Aerts, C., et al. 2011, *ApJS*, 197, 4
- Zhekov, S. A. 2014, *MNRAS*, 443, 12
- Zucker, S. 2003, *MNRAS*, 342, 1291. doi:10.1046/j.1365-8711.2003.06633.x